Analysis of air velocity distribution in a laboratory batch-type tray air dryer by computational fluid dynamics

D. A. Tzempelikos, A. P. Vouros, A. V. Bardakas, A. E. Filios, and D. P. Margaris

***Abstract*—**Batch dryers are some of the most widespread equipment used for fruit dehydration. Nevertheless, the optimization of the air distribution inside the drying chamber of a batch dryer remains a very important point, due to its strong effect on drying efficiency as well as the uniformity of the moisture content of the drying products. A new scale laboratory batch-type tray air (BTA) dryer was designed, constructed and evaluated for the drying of several horticultural and agricultural products. The airflow field inside the dryer was studied through a commercial computational fluid dynamics (CFD) package. A three-dimensional model for a laboratory BTA dryer was created and the steady-state incompressible, Reynolds-Averaged Navier-Stokes equations that formulate the flow problem were solved, incorporating standard and RNG k-ε turbulence models. In the simulation, the tray, used inside the BTA drying chamber, was modeled as a thin porous media of finite thickness. The simulations for testing the chamber were conducted at an average velocity of 2.9 m/s at ambient temperature. The CFD models were evaluated by comparing the airflow patterns and velocity distributions to the measured data. Numerical simulations and measurements showed that the new scale laboratory BTA dryer is able to produce a sufficiently uniform air distribution throughout the testing chamber of the dryer.

***Keywords*—** Airflow, Batch dryer, CFD, Simulation.

I. Introduction

ONE the most important factors in the designing of conventional batch-type air dryers is the airflow design. In industrial air dryers the effect of flow heterogeneity is particularly difficult to resolve. The distribution of airflow depends on the process of drying, the drying medium and the geometry of the drying chamber. These factors determine the uniformity of drying and thus the quality of the finished products. Even though the performance of a drying chamber can be studied experimentally, such a research restricts the generalization of the results and certainly cannot be applied to the original design of the drying chamber due to time and cost limitations. In contrast, with the help of computational fluid dynamics (CFD), which can span a wide range of industrial and non-industrial applications, the complexity of the flow field can be solved numerically.

Mathioulakis, Karathanos and Belessiotis [1] simulated the air flow in an industrial batch-type tray air dryer. The distribution of pressure and velocity over the product were found to lack in spatial homogeneity which led to variations in drying rates and moisture contents.

Margaris and Ghiaus [2] simulated the airflow in an industrial drier and provided parameters for different configurations that helped to optimize the drying space with significant improvement to the quality of the dried product and the reduction of energy consumption. Mirade [3] used a two-dimensional CFD model with time dependent boundary conditions, studying the distribution uniformity of air velocity in an industrial meat dryer for the low and high levels of a ventilation cycle. Hoang, Verbonen, Baerdemaeker and Nicolai [4] simulated the airflow inside a cold store solving the steady state incompressible, Reynolds-averaged Navier-Stokes (RANS) equations by applying the standard k-ε and the RNG k-ε turbulence models. The results showed that the RNG k-ε model does not improve the prediction of air recirculation whereas any improvements would require a finer grid with an enhanced simulation of a turbulent flow. Amanlou and Zomordian [5] designed a new fruit cabinet with various geometries and then simulated these geometries using CFD. The experimental results and the predicted data from the CFD revealed a very good correlation coefficient for the drying air temperature and the air velocity in the drying chamber. Norton and Sun [6] in a review paper demonstrated the widely use of CFD for predicting air velocity and temperature in drying chambers while Scott and Richardson [7] and Xia and Sun [8] presented the commercial CFD software that are being increasingly employed in the food industry.

Recent studies have shown that only a limited research on

D. A. Tzempelikos is PhD Student in the Fluid Mechanics Laboratory, Department of Mechanical Engineering and Aeronautics, University of Patras, GR-26500 Patras, GREECE (corresponding author, phone: +30-210-2896838; fax: +30-210-2896838; e-mail: dtzempelikos@meed-aspete.net).

A. P. Vouros is PhD Researcher in the Laboratory of Fluid Mechanics and Turbomachinery, Department of Mechanical Engineering Educators, School of Pedagogical and Technological Education (ASPETE), GR-14121 Athens, GREECE (e-mail: avouros@meed-aspete.net).

A. V. Bardakas is undergraduate student in the Laboratory of Fluid Mechanics and Turbomachinery, Department of Mechanical Engineering Educators, School of Pedagogical and Technological Education (ASPETE), GR-14121 Athens, GREECE (e-mail: abardakas@meed-aspete.net).

A. E. Filios is Professor in the Laboratory of Fluid Mechanics and Turbomachinery, Department of Mechanical Engineering Educators, School of Pedagogical and Technological Education (ASPETE), GR-14121 Athens, GREECE (e-mail: aefilios@meed-aspete.net).

D. P. Margaris is Associate Professor in the Fluid Mechanics Laboratory, Department of Mechanical Engineering and Aeronautics, University of Patras, GR-26500 Patras, GREECE (e-mail: margaris @mech.upatras.gr).

the prediction and measurements of flow and pressure fields in BTA dryers has been performed. The absence of experiments can be attributed to the difficulty of direct measurements of the local air velocity and flow into a drying chamber for horticultural and agricultural products.

The present study concerns the design, construction and evaluation of a new scale laboratory BTA dryer which can host thermal drying studies in fully controllable environment. The velocity and pressure fields are analyzed with the aid of the commercial CFD code Fluent®. For the numerical simulations, the steady state RANS equations are solved in combination with the standard k-ε and the RNG k-ε turbulence models. The effect of the k-ε and the RNG k-ε turbulence models is distinguished through direct comparisons of the derived airflow patterns. The purposes of the current research are: a) the study of the velocity fields in the drying chamber of a new scale laboratory BTA dryer while building a CFD method that is affordable in terms of computation time, and b) the comparison between the numerical results and the experimental measurements gathered with a velocity sensor.

II. Experimental Setup and Measurements

A. Description of the BTA dryer

The lab scale BTA dryer which has been designed and constructed in the Laboratory of Fluid Mechanics and Turbomachinery in ASPETE, is shown in Fig. 1 and 2. The overall dimensions of the facility are 4.7 m (length), 2.5 m (width) and 2.5 m (height). The air ducts are made from steel of 0.8 mm thickness. All the ducts are insulated with 10 mm Alveolen (Frelen) which has a thermal conductivity of 0.032 W/m·K and water absorption of 0.011 kg/m^2.

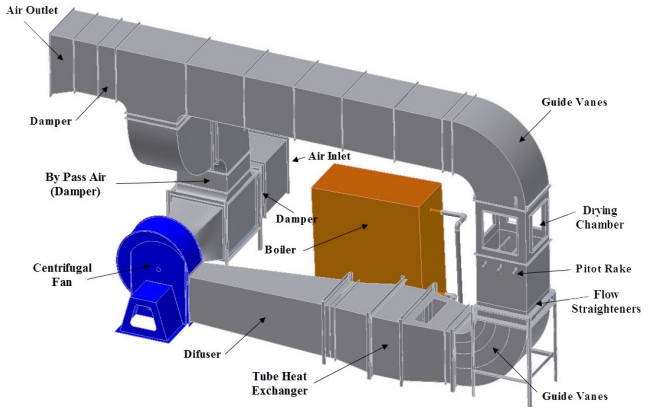

Fig. 1 Schematic diagram of the lab-scale BTA dryer

The square section drying chamber (0.5m x 0.5m) is of tower (vertical) type and is equipped with a metal tray which is supported on four, side wall-mounted, load cells. A set of four refractory glasses of 10 mm thickness are available to replace the side steel walls when optical clarity and precise visual observations are required.

Upstream of the drying chamber, the following parts are located: a long rectangular diffuser with a total divergence angle of 6.7 deg, a tube heat exchanger in which the hot water is provided through a boiler of 58 kW (50,000 kcal/h) thermal power, a transitional duct with observation window that includes a sprayer for humidifying purposes, a corner duct that incorporates four guide vanes and finally a flow straightener section. The flow straighteners, consisting of an aluminum honeycomb (made from 3003 aluminum alloy foil) with a cell size of 1/4' and 38 mm thickness and screen wires located downstream of the honeycomb, are considered necessary for flow uniformity in the drying section. The flow rate is observed and controlled with a custom made and calibrated rake of pitot tubes (namely pitot rake) located at the inlet of the drying chamber.

Downstream of the vertical drying chamber, the following parts are located: a second corner duct with guide vanes, an elevated horizontal modular constructed duct, an outlet dumper and an exit diffuser. The modular design of the facility permits the easy placement of two or three horizontal drying chambers in tandem arrangement, on the elevated return or exit flow leg.

The air flow is established and controlled through a centrifugal fan directly driven by a 3 phase electric motor of 3 kW with its speed regulated by an AC inverter. Adjusting the air dampers, the laboratory BTA dryer can be used for thermal drying experimental studies in both open circuit and close circuit operations.

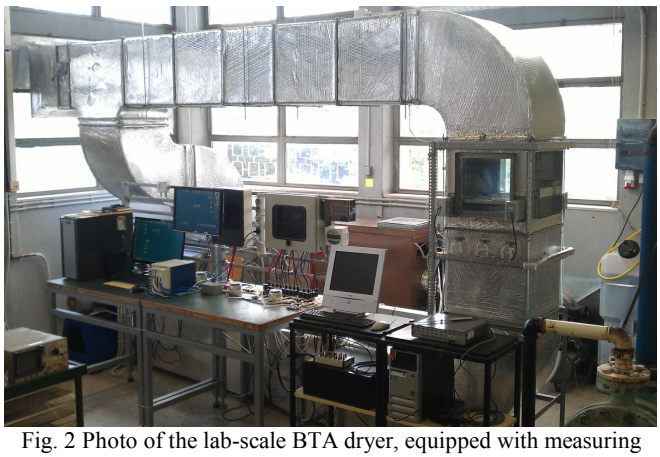

Fig. 2 Photo of the lab-scale BTA dryer, equipped with measuring instrumentation and data acquisition system

B. Measurements

The air velocity experiments inside the drying chamber, under ambient conditions, i.e. atmospheric pressure at 18.4 °C, were carried out with a constant speed of the induced centrifugal fan of 690 rpm at 23 Hz. The volumetric flow rate was 2,600 m^3/h, resulting to a mean velocity of 2.9 m/s and a Reynolds number of 9.9 x10^4 (based on the hydraulic diameter of the drying chamber).

The mean speed of the air flow at the inlet was the weighted average velocity of the 12 points collected from the pitot rake arrangement, as shown in Fig. 3, and the four pressure taps (same level with the contact tip of the pitot tube) on the side wall of the inlet of the drying chamber.

Each pitot tube is connected via plastic tubing to a custom

made pressure collector system equipped with solenoid valves (Tekmatic 24VDC, 6W) which allows its operation and control using a custom-made software developed in Labview®. A differential pressure transmitter (Dwyer, model MS-121-LCD) with a calibrated accuracy (± 2%) in the range of 25 Pa was used to measure each of the 12 points with an automatic "open-close" function of the proper solenoid valve.

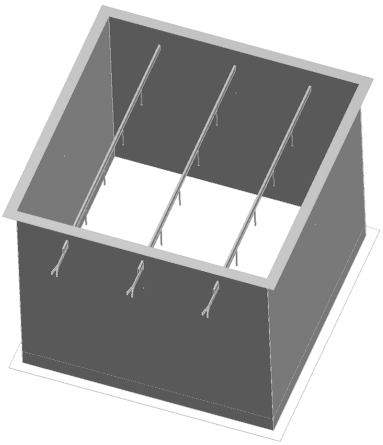

Fig. 3 The pitot tubes rake

For cross checking purposes of the pitot-static measured velocities, a velocity reference transducer (54T29, Dantec Dynamics® with 54N81 Multichannel CTA) was used, which offers the best value for cost and accuracy. The velocity range of the sensor is 0 – 30 m/s. The calibrated accuracy is ± 2% of reading ± 0.02 m/s or 2.6 % of the selected range of 3 m/s, which is assured by a certificate provided by the manufacturer.

The measurement of the velocity was done inside the duct at a distance of 0.51 m from the inlet of the drying chamber. In order to measure the air velocity during each test and at different locations of the drying chamber, 4 holes on the side wall of the drying chamber were pierced (Fig. 2 and 4). All holes, except the one through which the velocity transducer was inserted for the air velocity measurement, were filled tightly with conic plastic washers. The inlet air velocity was kept constant during the experiment.

In order to read the velocity at each point inside the drying cabinet, the velocity transducer was inserted through a side wall proximity hole and adjusted at eight different locations along the depth of the drying chamber. At each point the time averaged velocity was determined from the measurements which had a frequency of 200 Hz and averaged over a 10 second period. The experimental values were directly compared with the numerical predictions at the same locations.

Both the differential pressure transmitter and the velocity transducer were connected to a PC with the NI (National Instruments®) PCIe-6321 DAQ device via the NI SCXI-1000 and NI SCXI-1302 modules. Custom made software in Labview® was used to interface with the data acquisition.

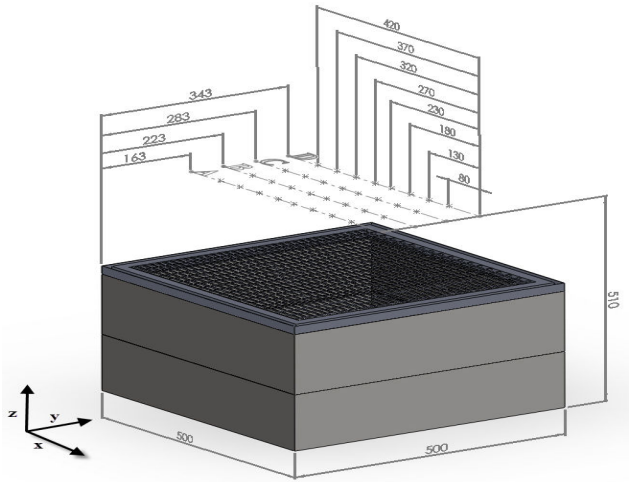

Fig. 4 A 3d view section of the drying chamber with the location of the measured velocities (dimensions in millimeters)

The overall accuracy of the CFD calculations is calculated as the average of the absolute differences between the time-averaged velocity magnitude for the CFD calculation and the measurement at each position, divided by the average velocity magnitude in the drying chamber obtained from the measurements and is expressed as:

$$E = \frac{\sum_{j=1}^{m} \left| U_{cfd}^{j} - U_{exp}^{j} \right|}{\sum_{j=1}^{m} U_{exp}^{j}} \times 100 \quad (1)$$

where U_{cfd}^{j} is the velocity at a position j for the CFD calculations, U_{exp}^{j} is the average velocity at a position j for the measurement and m is the number of measurement points.

III. Numerical Simulation

The numerical computation of fluid transport employs the conservation of mass, momentum and turbulence model equations. The Gambit® preprocessor was used to create geometry, to discretize the fluid domain into small cells that could form a volume mesh and to set up the appropriate boundary conditions. The flow properties could then be specified, the equations were solved and the results were analyzed using Fluent®.

A. Governing equations

The governing equations based on the conservation of mass and momentum of a Newtonian fluid flow, which apply to an infinitesimal small volume in a Cartesian co-ordinate system (x, y, z) using the Reynolds averaged formulation [9], are:

$$\frac{\partial \rho}{\partial t} + divU = 0 \quad (2)$$

$$\frac{\partial (\rho u_i)}{\partial t} + div(\rho U u_i) = div(\mu_{eff}\, gradu_i) - \frac{\partial p}{\partial x_i} + S_i \quad (3)$$

$$\rho = \rho(p, T) \quad (4)$$

$$\mu_{eff} = \mu + \mu_T \quad (5)$$

In these formulae, U is the velocity vector, consisting of three components u_x, u_y, u_z (m/s), p is the pressure (Pa) and T is the temperature (^oC). The density ρ (kg/m^3) and the laminar viscosity μ (N·s/m^2) are the only fluid properties involved; μ_T and μ_{eff} are the turbulent and effective viscosity, respectively. The S_i sources contain further contributions from the viscous stress term and may contain additional body forces. In all current calculations, constant air properties has been considered (ρ = 1.225 kg/m^3 and μ = 1.7894 x 10^{-5} N·s/m^2).

B. Turbulence models

The k-ε turbulence models are the most widely used and validated turbulence models in literature. The k-ε turbulence models use an eddy-viscosity assumption for the turbulence, expressing the turbulent stresses as an additional viscous stress term in (5). In the k-ε turbulence model, the turbulent viscosity is expressed in terms of two variables: the turbulence kinetic energy (TKE) k and the rate of dissipation of turbulent energy ε.

B.1 Standard k-ε turbulence model

The standard k-ε model which is valid only for fully turbulent flows, is a semi-empirical model based on model transport equations for the TKE k and its dissipation rate ε, containing empirical constants in the production and destruction terms of the ε equation. The model transport equation for the turbulence kinetic energy is derived from the exact equation, while the model transport equation for the dissipation rate is obtained using physical reasoning and bears little resemblance to its mathematically exact counterpart [10].

The resulting equations are similar to the governing flow equations [9]:

$$\mu_T = C_\mu \rho \frac{k^2}{\varepsilon} \tag{6}$$

$$\frac{\partial \rho k}{\partial t} + div(\rho U k) - div\left[\left(\mu + \frac{\mu_T}{\sigma_k}\right) grad(k)\right] = P - \rho\varepsilon \tag{7}$$

$$\frac{\partial \rho \varepsilon}{\partial t} + div(\rho U \varepsilon) - div\left[\left(\mu + \frac{\mu_T}{\sigma_\varepsilon}\right) grad(\varepsilon)\right] = C_{1\varepsilon}\frac{\varepsilon}{k}P - C_{2\varepsilon}\rho\frac{\varepsilon^2}{k} \tag{8}$$

where P is a term containing the turbulence production due to the stresses in the flow. The standard k-ε model contains five empirical constants (C_μ, $C_{1\varepsilon}$, $C_{2\varepsilon}$, σ_k and σ_ε) and during this study these constants remained the same:

$C_\mu = 0.09$, $C_{1\varepsilon} = 1.44$, $C_{2\varepsilon} = 1.92$, $\sigma_k = 1.0$ and $\sigma_\varepsilon = 1.3$ (9)

Near walls, the equations do not hold and standard logarithmic wall profiles have to be implemented. An important variable is y^+, a dimensionless distance normal to the wall. The value of y^+ determines in which region of the boundary layer the first node is situated. The log-law is valid only for $y^+ > 30$.

B.2 RNG k-ε turbulence model

The RNG (renormalization group) k-ε model employs a differential form of the relation for the effective viscosity, yielding an accurate description of how the effective turbulent transport varies with the effective Reynolds number. This allows accurate extension of the model to near-wall flows and low-Reynolds-number or transitional flows. Furthermore, a new term appears in the ε equation, which accounts for anisotropy in strongly strained turbulent flows. The same default wall functions as in the standard k-ε model are valid in this case as well. The ε equation is [9]:

$$\frac{\partial \rho \varepsilon}{\partial t} + div(\rho U \varepsilon) - div\left[\left(\mu + \frac{\mu_T}{\sigma_\varepsilon}\right) grad(\varepsilon)\right] = \left(C_{1\varepsilon} - C_{1RNG}\right)\frac{\varepsilon}{k}P - C_{2\varepsilon}\rho\frac{\varepsilon^2}{k} \tag{10}$$

$$C_{1RNG} = \frac{\left(1 - \frac{n}{n_0}\right)}{\left(1 + \beta n^3\right)} \tag{11}$$

$$n = \left(\frac{P_s}{\mu_T}\right)^{0,5}\frac{k}{\varepsilon} \tag{12}$$

where n_0 and β are additional model constants, which are equal to 4.38 and 0.012 respectively while P_s is the shear part of the production. The standard values of the other constants are considered suitable for this application:

$C_\mu = 0.0845$, $C_{1\varepsilon} = 1.42$, $C_{2\varepsilon} = 1.68$, $\sigma_k = 0.7179$ and $\sigma_\varepsilon = 0.7179$ (13)

The k equation has the same format as in the standard k-ε turbulence model.

C. Model of the tray

A source term was added to the k-ε and the RNG k-ε turbulence model equations to estimate the pressure drop across the tray inside the drying chamber. The tray was calculated as a screen and in the CFD simulation, the screen was modeled as a thin porous media of finite thickness over which the pressure change was defined as a combination of Darcy's Law and an additional inertial loss term which is given by [10]:

$$\Delta p = -\left(\frac{\mu}{\alpha}U_n + C_2\frac{1}{2}\rho U_n^2\right)\Delta m \tag{14}$$

where μ is the laminar fluid viscosity, α is the permeability of the tray, C_2 is the pressure-jump coefficient (pressure loss coefficient per unit thickness), U_n is the velocity normal to the tray, and Δm is the thickness of the tray.

D. Model of the BTA dryer

The flow field inside the drying chamber of an empty laboratory BTA dryer, operated in open circuit mode was numerically studied. The structure of the modeled dryer is depicted in Fig. 5. The dryer is 4.7 m in length, 0.5 m in width and 1.38 m in height. The dimensions of the drying chamber are 0.5 x 0.5 x 0.66 m.

The BTA dryer is modeled with the tray located in a distance of 0.29 m from the inlet of the drying chamber. The tray has a length of 0.48 m, a width of 0.48 m and a thickness

of 2.8 mm. The shape of the tray has been modeled as a screen with orthogonal holes. The dimensions of the orthogonal holes are 23.7 mm x 10.9 mm. A gap of 10 mm exists between the tray and the wall of the drying chamber.

The velocity profile at the entrance of the drying chamber was measured by using 12 points (Fig. 3). These points were used as an inlet boundary condition for the simulation performed and for that reason the geometry of the fan, the diffuser, the tube heat exchanger, the down guide vanes and the flow straighteners were not modeled.

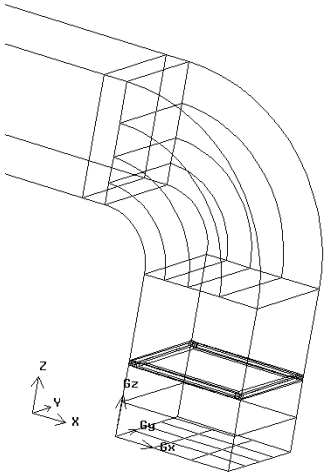

Fig. 5 3d wire frame view of the BTA drying chamber with tray

E. Description of the numerical simulation

The calculations were performed with Fluent®. In the steady RANS simulations of the airflow into the BTA dryer, the standard k-ε and the RNG k-ε turbulence models were used. In the derivation of the k-ε model, it was assumed that the flow was fully turbulent, and the effects of the molecular viscosity were negligible. The standard logarithmic wall functions, which are a collection of semi-empirical formulas and functions were applied to bridge the viscosity affected region between the wall and the fully turbulent region. The SIMPLE algorithm was used alongside the solver of Fluent®, to solve the pressure-velocity coupling equations. In order to improve the numerical accuracy, the second-order-upwind scheme was used to discretize the RANS equations.

F. Numerical solution control

For the numerical simulations, a desktop PC (Intel® Core i7 CPU at 2.67 GHz) was used. The number of iterations was adjusted to reduce the scaled residual below the value of 10^{-5} which was the criteria. For each run, the observation of the integrated quantities of total pressure, at the suction as well as at the discharge surface was used for the convergence of the solution. In many cases, this can push the residuals to lower values than the initially set value. Depending on the case, the convergence was achieved at difference iterations, as the result at a specific mass-flow was used to initialize the computations at another mass-flow. Aiming for a smooth convergence, various runs were performed by varying the under-relaxations factors. In that way, direct control, regarding the update of computed variables through iterations, was achieved. Initializing with low values for the first iteration steps and observing the progress of the residuals, the values were modified in order to accelerate the convergence.

G. Boundary conditions and mesh cells

The inlet boundary condition of the model was set as an inlet velocity profile by using a set of velocities, measured at 12 points inside the air dryer (Fig. 3). The direction of the velocity was normal to the inlet boundary and the average velocity was 2.89 m/s. The turbulent intensity, which is defined as the ratio of the root-mean-square of the velocity fluctuations, to the mean flow velocity can be estimated from the following formula derived from an empirical correlation for pipe flows [10],

$$I = \frac{u'}{u_{avg}} = 0{,}16\left(Re_{Dh}\right)^{-1/8} \tag{15}$$

The turbulent intensity at the inlet boundary was set as 3.8%, for a Re = 9.9 x 10^4. An atmospheric pressure boundary located downstream of the outlet duct was specified as the pressure outlet. The no-slip boundary condition was used for all the walls. The porous jump boundary condition was used for the tray, and appropriate values for the pressure jump coefficient, C_2, and the permeability α, were calculated from the literature [11].

The CFD model of the new scale laboratory BTA dryer consisted of about 800000 computational nodes (Fig. 6). A body fitted structured grid was used. The grid was refined for when it was close to the walls, in between the wall and the tray and inside the tray. The y^+ was in the range of 30 to 50. The grid independence was checked and a converged solution was obtained after approximately 1900 iterations.

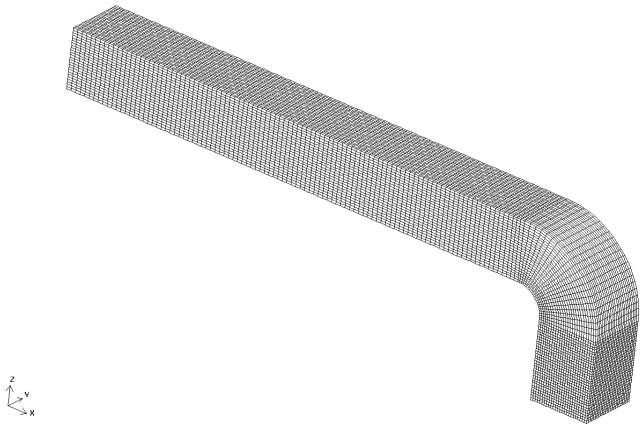

Fig. 6 Computational grid of the air dryer model

IV. Results and Discussion

The predicted velocities using the k-ε and RNG k-ε models for a height z = 0.51 m, as shown in Fig. 4, were compared with the corresponding experimental values. Fig. 7a to 7d shows a comparison between the measured and the simulated values of the air velocity distribution, which gives the overall accuracy of the CFD calculations, E in (1), 2.79 % for the k-ε and 2.72 % for the RNG k-ε turbulence model.

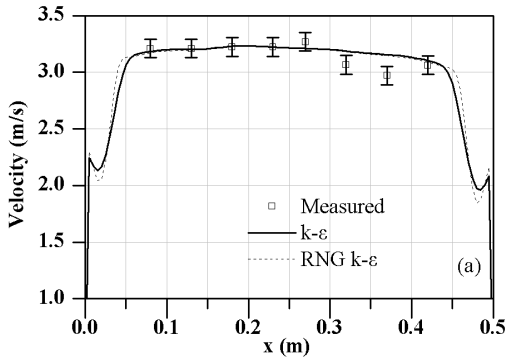

(a) z = 0.51 m, y = 0.163 m

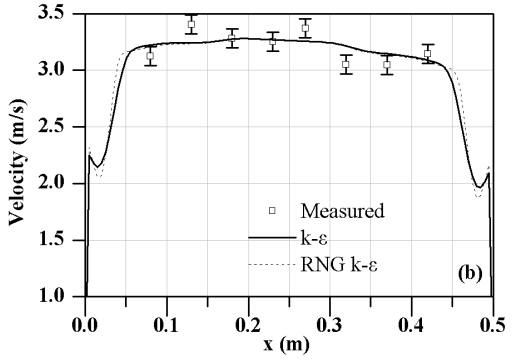

(b) z = 0.51 m, y = 0.223 m

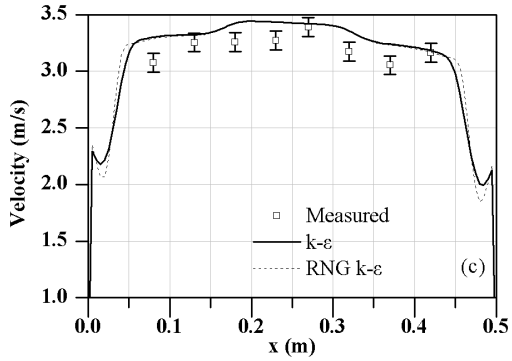

(c) z = 0.51 m, y = 0.283 m

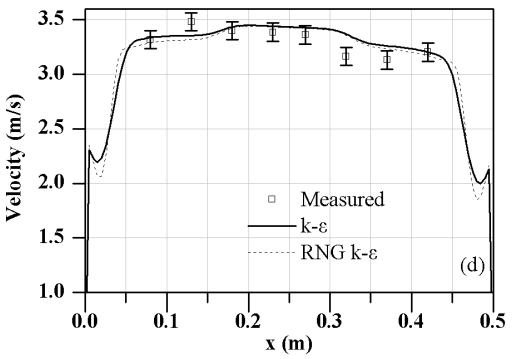

(d) z = 0.51 m, y = 0.343 m

Fig. 7 Velocity field measurements compared with CFD predictions in the BTA drying chamber

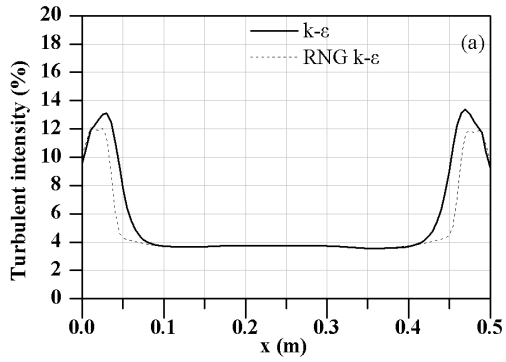

(a) z = 0.51 m, y = 0.163 m)

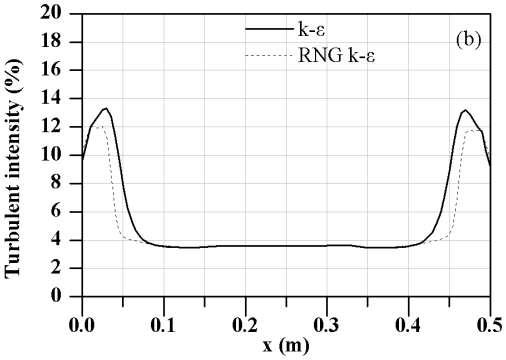

(b) z = 0.51 m, y = 0.223 m

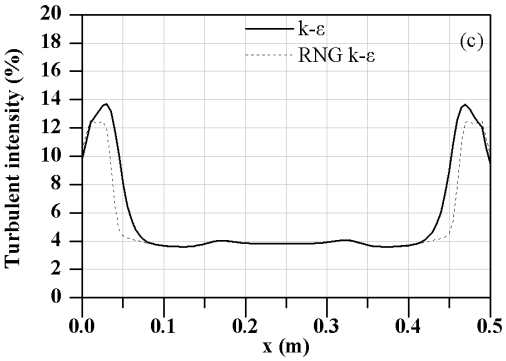

(c) z = 0.51 m, y = 0.283 m

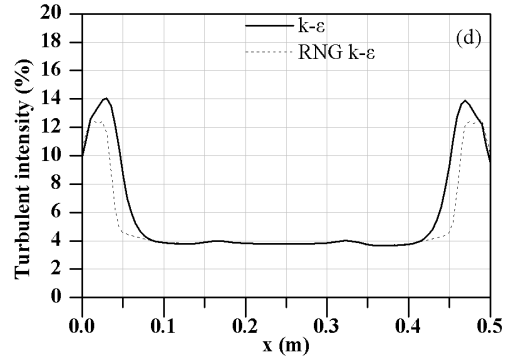

(d) z = 0.51 m, y = 0.343 m

Fig. 8 Turbulent intensity predictions and comparisons in the BTA drying chamber

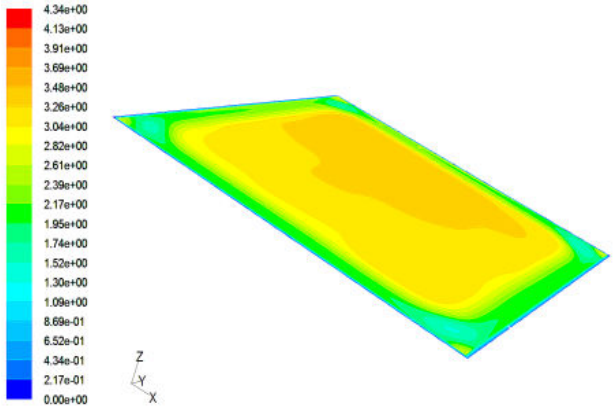

(a) k-ε turbulence model

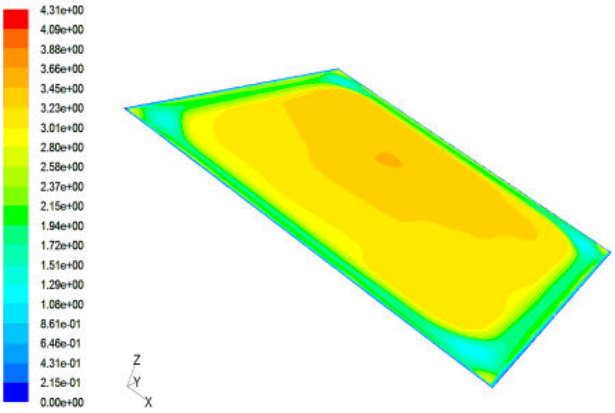

(b) RNG k-ε turbulence model

Fig. 9 Velocity contours (m/s) in BTA drying chamber cross section (z = 0.51 m)

The difference of the absolute between the simulated and experimental values varied from 0.002 to 0.227 m/s for the k-ε and from 0.002 to 0.213 m/s for the RNG k-ε turbulence model.

The relative error between the simulated and experimental values varied from 0.08 to 7.38 % for the k-ε and from 0.08 to 6.93 % for the RNG k-ε turbulence model.

The average velocity of the experimental values was 3.22 m/s with a standard deviation of 0.12761. The average velocity and standard deviation for the k-ε and RNG k-ε turbulence models were 3.274 m/s, 0.09367, 3.267 m/s and 0.10503 respectively.

The overall accuracy of the CFD calculations indicates that the CFD simulation scheme is practical for the analysis of the velocity field in the drying chamber.

Fig. 8a to 8d illustrates the turbulent intensity predicted with the k-ε and the RNG k-ε models at the position z = 0.51m. The average turbulent intensity was about 4%. At the edges of the drying chamber (0.05 m for the wall) the turbulent intensity reached almost 14%. This difference can be explained by the presence of the tray and its geometry.

In Fig. 9a to 9b, the velocity contours which were chosen for their relevance concerning the assessment of the airflow calculations are shown. It can be seen that high velocities are encountered at the center of the chamber.

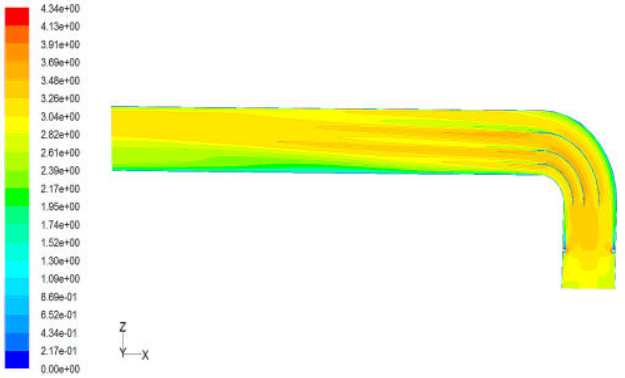

(a) k-ε turbulence model

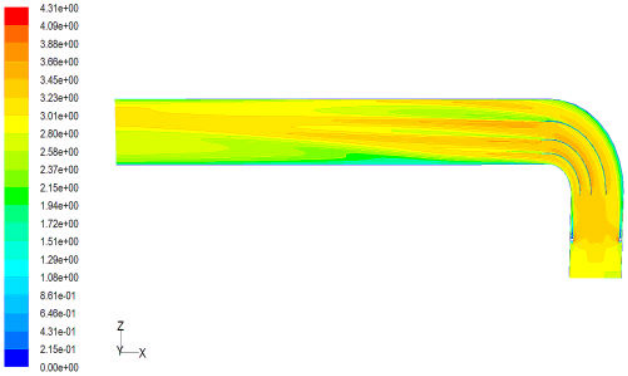

(b) RNG k-ε turbulence model

Fig. 10 Streamwise velocity magnitude contours (m/s) in y = 0.25 m plane

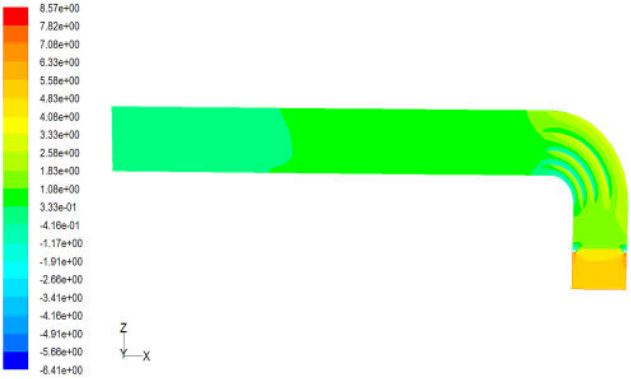

(a) k-ε turbulence model

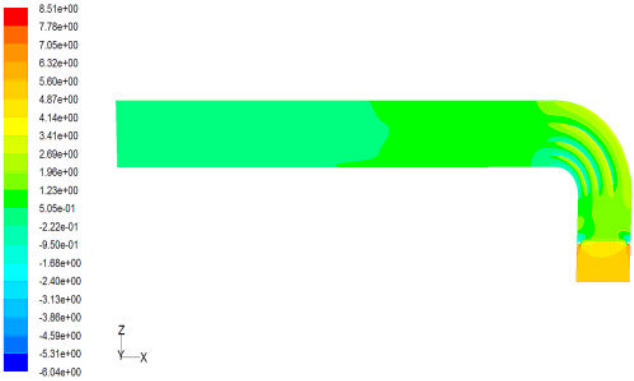

(b) RNG k-ε turbulence model

Fig. 11 Streamwise static pressure contours (Pa) in y = 0.25 m plane

Near the four walls the air moves at lower velocities due to the presence of the tray which was located 0.2 m below the level of where the measurements were taken. Both turbulence models predict almost the same air flow distribution.

Fig. 8a to 8d and 9a to 9b verify that at the core of the drying chamber, the turbulent intensity of the velocity field is relatively low and the flow is homogenous.

The stream wise velocity contours of the BTA dryer are presented in Fig. 10a and 10b. The velocity contours reveal the presence of high velocity regions especially at the middle of the drying chamber and above the tray disk.

In Fig. 11a and 11b, the static pressure contours in the air dryer reflect the presence of a low velocity regime, especially at the inlet of the drying chamber and at the upper guide vanes. At a distance of 310 mm from the inlet of the drying chamber, there is a pressure drop from 6 to 1 Pa in terms of gauge pressure. This drop of the static pressure is due to the presence of the tray disk at this location.

In Fig. 12, δ represents the relative difference of the velocity magnitude of the k-ε and the RNG k-ε turbulence models with respect to the k-ε turbulence model and is defined as:

$$\delta = \frac{U^i_{k-\varepsilon} - U^i_{RNG\,k-\varepsilon}}{U^i_{k-\varepsilon}} \times 100 \qquad (16)$$

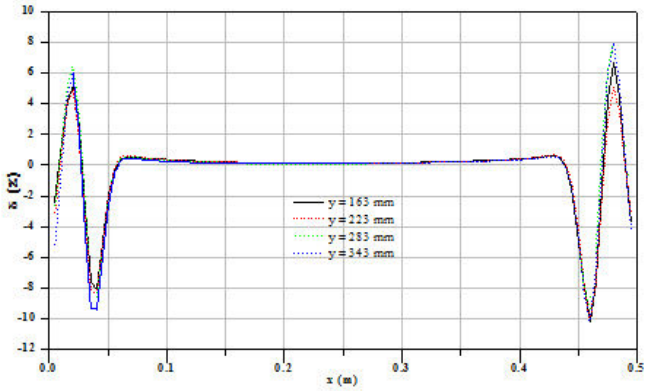

Fig. 12 Relative differences in the computed velocities at four y-planes applying k-ε and RNG k-ε turbulence models

Near the wall of the drying chamber the parameter δ reaches almost 10% whilst in the middle of the chamber, the velocity predictions are independent of the turbulence model.

V. Concluding Remarks

A fluid flow model of a new scale laboratory BTA dryer, including its major physical features, was developed using CFD code Fluent®. Standard k-ε and RNG k-ε turbulence models were used for computing the turbulence parameters inside the air dryer. Numerically predicted velocity profiles inside the drying chamber were compared with the measured data. These predictions were found to be in reasonable agreement with the measured data. The turbulence intensity was low and the homogeneity of the drying chamber was acceptable. There was a slightly difference between the k-ε and the RNG k-ε turbulence models predicting the velocity profiles, however the model developed was found to be useful for predicting the airflow pattern inside the drying chamber. Further work will focus on validating the CFD results with drying experiments using organic and inorganic products in the drying chamber of the air dryer.

Nomenclature

E	Average difference between the measured and the predicted velocities (%)
U^j_{cfd}	Predicted velocity at position j (m/s)
U^j_{exp}	Average measured velocity at position j (m/s)
m	Number of measurement points
U	Velocity vector (m/s)
t	Time (s)
u	Velocity component (m/s)
p	Pressure (Pa)
S	Source term in momentum equation (N/m^3)
T	Temperature (^{o}C)
C_μ	Constant in the turbulent viscosity equation
k	Turbulence kinetic energy (m^2/s^2)
P	Turbulence energy production (kg/m·s^3)
$C_{1\varepsilon}$	Constant in the production term of the ε equation
$C_{2\varepsilon}$	Constant in the dissipation term of the ε equation
y^+	Dimensionless normal distance to the wall
C_{1RNG}	Constant in the production term of the ε equation in the RNG k-ε model
n	Term in the ε equation of the RNG k-ε model
n_0	Constant in the ε equation of the RNG k-ε model
P_s	Shear part of turbulence energy production (kg/m·s^3)
U_n	Velocity normal to the tray face (m/s)
C_2	Pressure jump coefficient (m^{-1})
I	Turbulent intensity (%)
u'	Fluctuating velocity (m/s)
u_{avg}	Average velocity (m/s)
Re	Reynolds number
$U^i_{k-\varepsilon}$	Predicted velocity at position i for the k-ε model (m/s)
$U^i_{RNG\,k-\varepsilon}$	Predicted velocity at position i for the RNG k-ε model (m/s)

Greek symbols

ρ	Density (kg/m^3)
μ	Viscosity (N·s/m^2)
μ_T	Turbulent viscosity (N·s/m^2)
μ_{eff}	Effective viscosity (N·s/m^2)
ε	Turbulence energy dissipation (m^2/s^3)
σ_k	Turbulent Prandtl number for k

σ_ε Turbulent Prandtl number for ε
β Constant in the ε equation of the RNG k-ε model
Δp Pressure drop across the tray (Pa)
α Permeability of the tray (m^2)
Δm Thickness of the tray (m)
δ Relative difference between the k-ε and the RNG k-ε predicted velocities (%)

Subscripts
i index of Cartesian components
Dh *Hydraulic diameter*

ACKNOWLEDGMENTS

The measuring equipment and the data acquisition of the lab-scale BTA dryer in the Laboratory of Fluid Mechanics and Turbomachinery was partially funded by public and private sponsors. The authors gratefully acknowledge the Special Account for Research of ASPETE, Delta Pi S.A., A.A. Roibas & Co., Mr. Dionisios Tsepenakas (EKO S.A.) and Mr. Michalis Petrolekas (National Instruments, Hellas) for their kind contribution and support.

REFERENCES

[1] E. Mathioulakis, V. T. Karathanos, and V. G. Belessiotis, "Simulation of air movement in a dryer by computational fluid dynamics: Application for the drying if fruits", Journal of Food Engineering, Vol. 36, pp. 183-200, 1998.
[2] D. P. Margaris and A. G. Ghiaus, "Dried product quality improvement by air flow manipulation in tray dryers", Journal of Food Engineering, Vol. 75, pp. 542-550, 2006.
[3] P. S. Mirade, "Prediction of the air velocity field in modern meat dryers using unsteady computational fluid dynamics (cfd) models", Journal of Food Engineering, Vol. 60, pp. 41-48, 2003.
[4] M. L.Hoang, P. Verbonen, J. Baerdemaeker and B. M. Nicolai, "Analysis of the air flow in a cold store by means of computational fluid dynamics", International Journal of Refrigeration, Vol. 23, pp. 127-140, 2000.
[5] Y. Amanlou, and A. Zomordian, "Applying CFD for designing a new fruit cabinet dryer", Journal of Food Engineering, Vol. 101, pp. 8-15, 2010.
[6] T. Norton and D. W. Sun, "Computational fluid dynamics (CFD) – an effective and efficient design and analysis tool for the food industry: a review", Trends in Food Science and Technology, Vol. 17, pp. 600-620, 2006.
[7] G. Scott and P. Richardson, "The application of computational fluid dynamics in the food industry", Trends in Food Science and Technology, Vol. 8, pp. 119-124, 1997.
[8] B. Xia and D. W. Sun, "Applications of computational fluid dynamics (CFD) in the food industry: a review", Computers and Electronics in Agriculture, Vol. 34, pp. 5-24, 2002.
[9] J. Tu, G. H. Yeoh and C. Liu, *Computational Fluid Dynamics, A Practical Approach*, 1st ed., Butterworth-Heinemann, 2008.
[10] Fluent 6.3 User's Guide, Fluent Inc., 2006.
[11] I. E. Idelchik, *Handbook of hydraulic resistance*, 3rd ed., CRC Press Inc., 1994.